journal

J. Am. Ceram. Soc., **86** [2] 333–41 (2003)

Grinding Temperature Measurements in Magnesia-Partially-Stabilized Zirconia Using Infrared Spectrometry

Adam C. Curry

Department of Mechanical and Aerospace Engineering, North Carolina State University, Raleigh, North Carolina 27695

Albert J. Shih

Department of Mechanical Engineering, University of Michigan, Ann Arbor, Michigan 48109

Jin Kong

Department of Mechanical and Aerospace Engineering, North Carolina State University, Raleigh, North Carolina 27695

Ronald O. Scattergood**

Department of Materials Science and Engineering, North Carolina State University, Raleigh, North Carolina 27695

Sam B. McSpadden

High Temperature Materials Laboratory, Oak Ridge National Laboratory, Oak Ridge, Tennessee 37831

Results of temperature measurements by analysis of the thermal emission spectra generated during grinding and subsequently transmitted through partially stabilized zirconia workpieces are presented. Portions of emitted visible and near-infrared spectra were collected with spectrometers. Source temperatures were determined by fitting the scaled spectrometer output spectra to blackbody curves. Simulations showed that the effective temperatures determined by this method will be strongly biased toward hot-spot (flash) temperatures, which are expected to occur at the grinding grit–workpiece interface. Hot-spot temperatures on the order of 3000 K were obtained for grinding with both SiC and diamond wheels. These high temperatures modify the grinding process and the phase content of grinding chips.

I. Introduction

HEAT generation is an important factor for the grinding of ceramics. It can degrade the integrity of the wheel matrix and/or abrasive, reduce workpiece surface quality by causing thermal cracks or burning of the surface, introduce strength-reducing tensile residual stresses, and create dimensional inaccuracies. Temperature may also influence the grinding mechanism, either by softening the material or by introducing phase transformations.[1–3]

Although thermocouples are ideal for many temperature-measurement applications, they are severely limited for measuring grinding temperatures. Their shortcomings lie in their poor spatial and temporal resolutions. Resolution is dictated by the size of the hot junction, the time response of the thermocouple, and the conductivity through the workpiece. Furthermore, the low thermal conductivity of ceramics requires that any contacting temperature measurement device be placed so close to the grinding zone that it will likely be destroyed before an accurate temperature can be obtained. These difficulties make noncontact fast time-response methods, such as infrared emission spectroscopy, more suitable for grinding temperature measurement.

A number of researchers have undertaken the task of determining the temperatures generated during grinding. The majority of temperature measurement methods reported to date can be divided into the following categories: “blind-hole,” “through-hole,” “wheel-surface,” and “grinding-interface.” In assessing the different methods, it is important to note the difference between single-wavelength and multiple-wavelength methods. So-called “single-wavelength” methods measure the intensity of the spectral output without discriminating between different wavelengths. Calibration techniques are needed so that the absolute value of the measured intensity can be correlated with source temperature. This requires knowledge of the emissivity of the source as well as all other parameters that modify intensity between source and detector. In contrast, so-called “multiple-wavelength” techniques use the ratio of two or three intensities at specific wavelengths to determine temperature in conjunction with blackbody radiation curves. As long as emissivity and other parameters are independent of wavelength over the measurement range, these do not have to be determined independently. Spectrometer methods determine the intensity spectrum from the source over a wavelength range and fit this to blackbody curves to determine temperature, again assuming that all relevant parameters are independent of wavelength.

J. R. Hellmann—contributing editor

Manuscript No. 187568. Received July 23, 2001; approved June 17, 2002.

Portions of this research were sponsored by the User program of the High Temperature Material Laboratory, Oak Ridge National Laboratory. This project was also supported by the National Science Foundation (Dr. K. P. Rajurkar, Program Director).

**Fellow, American Ceramic Society.

Spectrometer methods have the advantage that spurious effects such as triboluminescence peaks should be detectable in the spectral output.

Blind-hole methods[4–6] involve measurement of the temperature below the grinding surface. This is done by monitoring the temperature at the upper surface of a blind hole drilled into the workpiece from the bottom. Temperature is monitored as the distance from the measured surface to the grinding surface decreases with subsequent passes of the wheel. Until the distance of the measurement from the grinding surface is very small, approximately on the order of the distance between individual grinding grits, conduction effects dictate that the temperature of individual grits cannot be resolved. Extrapolated temperatures represent an uncertain average value. Through-hole methods[7–9] involve the observation of radiation emitted by the wheel and passing through a hole in the workpiece. Depending on the geometry and the type of measurement method used, peak temperatures can be measured. Peak temperatures from individual asperity contacts have been determined using high spatial resolution detectors.[7] The wheel-surface method[10] provides wheel temperatures at various points about the grinding wheel periphery. An average surface temperature is measured in this case. With the grinding-interface methods, temperatures are measured within the grinding zone and at asperity contacts in pin-on-disk rubbing. The grinding study presented by Outwater and Shaw[11] employs a thermocouple method in which dissimilar metals are smeared across the grinding surface by the wheel. This method, which provides the average temperature across the smeared region, does not measure hot-spot temperatures. Chandrasekar and coworkers[7,9] and Griffioen *et al.*[12] have developed grinding-interface methods pertinent to this study. In their studies, asperity peak temperatures were estimated for single-point cutting/sliding or full-wheel grinding. The infrared transmission through a transparent workpiece was used for the measurements reported by Griffioen *et al.*[12]

II. Thermal Effects in Grinding

The grinding process is best understood by considering it on global and local scales. Distinctions between the two are particularly important in discussing grinding temperature.

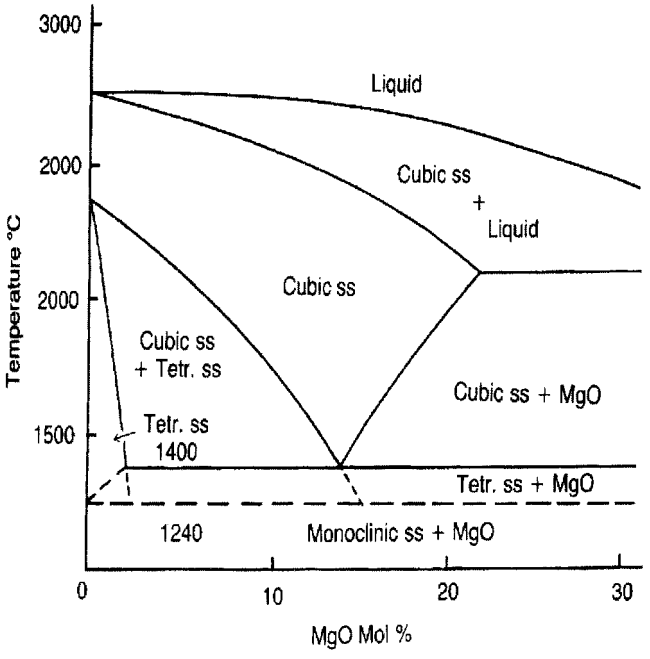

Fig. 1. Phase diagram for MgO-PSZ.[19]

When a grinding grit engages the workpiece, it first causes deformation. This stage is known as plowing. If the stress level becomes great enough, chip formation begins. Finally, the chip breaks loose and is carried out of the grinding zone by grinding fluid. The fluid serves both to remove chips, collectively known as swarf, and to cool the workpiece. Cooling is often critical in grinding because a significant amount of heat is typically generated in the process. Heat is generated primarily by three actions. First is shearing or fracture of the workpiece during chip formation. Second is the friction of the chip sliding at the grit's rake face. Lastly, heat is generated along the portion of the grit worn flat either by truing or by previous passes through the workpiece. Heat generated by any of these means, when it is localized near the grit or in the chip, is known as hot-spot (flash) temperature. Each grit acts as an asperity heat source, with conduction serving to distribute the heat from individual grits and raise the overall temperature of the grinding surface.[5,7] The temperature far from the grits is known as the background temperature. As would be expected, and as some researchers have shown, the values of these temperatures typically differ substantially, especially in materials with low thermal conductivity, such as ceramics.

The defining characteristic of transformation-toughened ceramics, such as the partially stabilized 9-mol%-MgO-partially-stabilized zirconia (MgO-PSZ) used for this study, is the introduction of a metastable phase. The effects occurring during grinding can be viewed in terms of the MgO-PSZ phase diagram shown in Fig. 1. After appropriate heat treatment,[13] the cubic (*c*), monoclinic (*m*), and tetragonal (*t*) phases are present at room temperature. The *c* and *t* phases are metastable at room temperature. Stress will drive the $t \rightarrow m$ martensitic transformation that increases toughness. Increasing temperature can also transform both *c* and *t* phases to the stable *m* phase. Above 1513 K (1240°C) the *m* phase will become unstable, and at even higher temperatures only *c* and liquid phases will be stable. The thermomechanical history during grinding is complex since there will be a rapid increase in both stress and temperature at the grit–workpiece interface followed by a rapid quench in grinding coolant. Analysis of the phases present before and after grinding, in both chips and ground surfaces, gives some indication of the history. However, the picture is limited since conventional X-ray diffraction techniques can distinguish the amount of *m* phase and $c + t$ phases present, but not the individual amounts of the *c* and *t* phases.

The grinding performance of the PSZ material used in this study was investigated in detail in several companion studies.[14–16] SiC and diamond-grinding wheels were used on two different machines for a systematic investigation of grinding behavior. When the grinding wheel specifications are properly chosen, a SiC grinding wheel performs remarkably well for grinding PSZ. Diamond grinding wheels have been the traditional choice for these and most other structural ceramics. Rather surprisingly, the highest *G* ratios are obtained at higher grinding rates for the SiC wheel. This, and the fact that SiC grinding wheels can be readily shaped for use in precision cylindrical form grinding, have been exploited for cost-effective production of PSZ components in automotive applications. Several important effects were noted in the companion study. X-ray diffraction showed that the *m* phase was not present in any of the grinding chips when SiC wheels were used. Some *m* phase was retained in the chips with diamond wheels. In contrast, the ground surfaces contained excess, relative to virgin surfaces, of the *m* phase. Thermal conductivity must play a role in these effects. The thermal conductivity is ~2, 150, and 2000 $W \cdot m^{-1} \cdot K^{-1}$ for zirconia, SiC, and diamond, respectively. Very low thermal conductivity for zirconia will help retain heat and raise temperature, especially in grinding chips, which have restricted volume. High chip temperatures, as well as stresses, would modify the phases present after grinding. High temperatures at the grit–workpiece interfaces could also locally soften or even partially melt the PSZ. These issues motivated the current investigation for the determination of

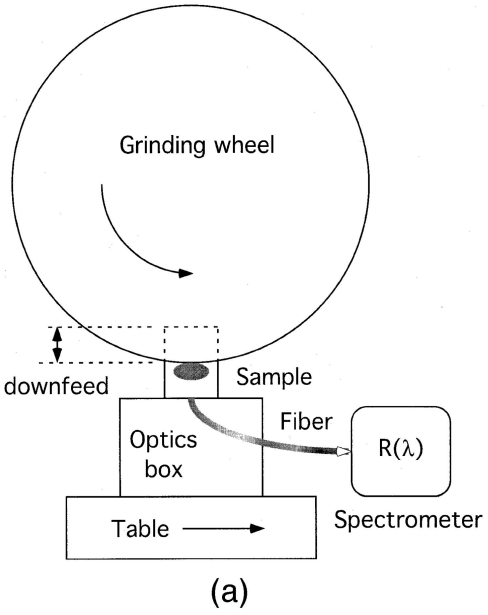

(a)

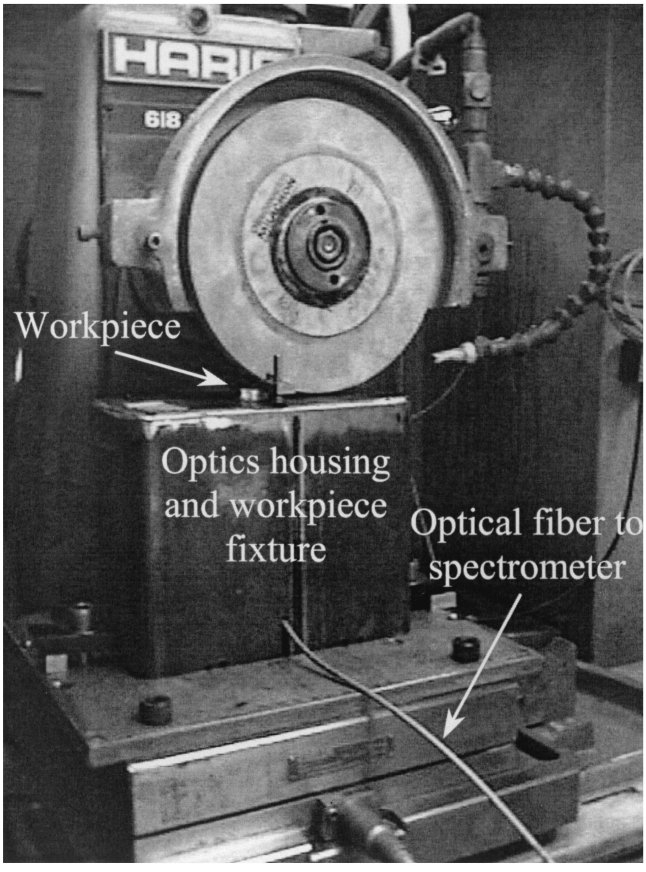

(b)

Fig. 2. (a) Schematic of the grinding test setup. (b) Photograph of the setup.

grinding temperatures using PSZ workpieces with SiC and diamond wheels. An advantage of PSZ is the fact that it is semitransparent in the near-infrared and light transmitted through the workpiece can be collected. For the method implemented here, it was possible to make measurements in the presence of grinding coolant, so that the results reflect the conditions present in real grinding processes.

Several previous studies support the hypothesis for high temperatures at the grit–workpiece interface during grinding of zirconia. Using a three-wavelength technique, Hebbar *et al.*[7] reported single-point and full-wheel peak temperatures on the order of 1600 to 1900 K for zirconia. In their studies of abrasive behavior of zirconia, Costa *et al.*[2] and Swain and Hannink[3] report that the temperature generated during abrasive processes can counteract the stress-induced transformation, $t \rightarrow m$, by producing the reverse transformation $m \rightarrow t$ above 1513 K (Fig. 1). Swain and Hannink[3] also note that the temperatures at the interface in grinding should be substantially elevated because of the low thermal conductivity of zirconia. Although zirconia was not tested, Griffioen *et al.*[12] used an infrared camera transmission technique and reported peak temperatures as high as 3000 K for single-point contacts of silicon nitride pins sliding on a transparent sapphire workpiece.

III. Experimental Procedure

Grinding tests were done on a Harig surface grinder. The table speed was fixed at 150 mm/s. The wheel speeds used were 3500, 4000, and 4500 rpm (37, 42, and 47 m/s surface cutting speed, respectively). Downfeeds, i.e., nominal depths of cut (Fig. 2(a)), were 0.0025, 0.005, and 0.0075 mm. Specimen thickness depended on the number of prior grinding passes, and these varied from about 0.1 to 1.3 mm. Two grinding wheels were used. The first was a specially selected 220 ANSI mesh SiC grit vitreous bond wheel[16] while the second was a 220 ANSI mesh diamond grit resin bond wheel. Both wheels measured 200 mm in diameter with a width of 10 mm. Water-based Cimtech 500 synthetic coolant at 5% concentration was used during grinding. Sample fixturing and other details of the grinding procedure are given in.[15] The workpiece material used for all grinding tests was 9 mol% MgO-PSZ supplied by Coors.

Temperature measurements were conducted with two different spectrometers. All of the test results reported here were obtained using an Ocean Optics USB2000 near-infrared (0.717 to 0.980 μm wavelength range) spectrometer. For comparison, selected tests were also done using an Ocean Optics S2000 visible (0.191 to 0.853 μm wavelength range) spectrometer. Ocean Optics spectrometers take advantage of charge-coupled discharge (CCD) arrays to allow for acquisition of an entire spectrum over one sampling time. Furthermore, they are relatively inexpensive and can be readily integrated with a data acquisition system. As seen in the schematic of the test setup in Fig. 2(a), light transmitted through the PSZ workpiece is collected and fed to a 600 μm diameter multimode optical fiber which is carried to the spectrometer aperture for intensity measurements. A common problem in using optical fibers for temperature measurement is the signal attenuation that can result from changes in the fiber's orientation. However, as long as there is no spectral variation in the attenuation, it does not affect the spectrometric measurement method used here. Furthermore, when a steady source was used to check the fibers for signal attenuation due to movement of the fiber, none was observed. The actual test setup implemented on the grinding machine is shown in Fig. 2(b). The cable running from the optics housing passes the light to the spectrometer (not shown). The measurement signal can be captured only when the moving workpiece on the table passes under the grinding wheel (Fig. 2(a)); therefore, the measurement-time window is limited by the grinding table speed (150 mm/s) and the sample size (20 mm × 20 mm × 6.35 mm). Typical data collection times were on the order of 60 ms or less.

The spectrometers must first be calibrated to a known temperature source to obtain accurate spectra. Calibrating the spectrometer sets each pixel in its CCD array to the appropriate gain. This ensures that the relative intensities of each wavelength are correct, so the spectra shapes accurately indicate the source temperatures. Three sources were used for initial calibration and for verification of the calibrations: a tungsten halogen lamp at 3100 K and blackbody ovens at 1273 and 2773 K. Spatial resolution of the system shown in Fig. 2 was insufficient to resolve individual grinding grits; therefore, the field of view will contain multiple

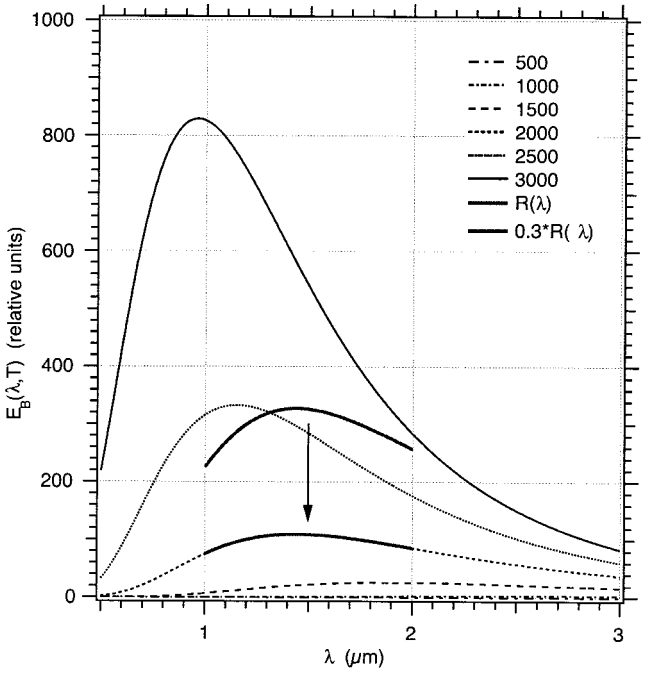

Fig. 3. Blackbody radiation curves for the temperatures indicated. Scaling (vertical shift) of the $R(\lambda)$ spectral data produces a best fit for 2000 K, as indicated.

grinding grit contacts (hot spots) distributed over a background, like stars in a night sky. As will be discussed further, the temperatures measured using the spectrometer method must be interpreted with the aid of simulations.

IV. Analysis Method and Results

Multiple-wavelength techniques use relative intensities at different wavelengths to determine an effective (graybody) source temperature. For the spectrometer method used here, this was done by matching the scaled spectrometer output, $R(\lambda)$, to blackbody curves, $E_B(\lambda,T)$, over the measurement wavelength range. This is illustrated schematically in Fig. 3. The $R(\lambda)$ data are scaled (shifted vertically) and simultaneously matched with $E_B(\lambda,T)$ curves until the best fit with one of the blackbody curves is obtained. For example, in Fig. 3 the output $R(\lambda)$, taken over the measurement range 1 μm $\leq \lambda \leq$2 μm, fits best to the 2000 K blackbody curve using a scaling factor of 0.3. The effective graybody source temperature determined from the $R(\lambda)$ spectrum is thus 2000 K.

The equation used for the data analysis method is based on the blackbody radiation equation plotted in Fig. 3,

$$E_B(\lambda,T) = \frac{C_1}{\lambda^5(e^{C_2/\lambda T} - 1)} \tag{1}$$

$C_1 = 8\pi hc = 4.992 \times 10^{-24}$ N·m^2 and $C_2 = hc/k = 14390$ μm·K where h, k, and c are Planck's constant, Boltzmann's constant, and the velocity of light, respectively. For radiation at temperature T from a source of emissivity ε passing through a material with transmissivity τ into a spectrometer with an aperture constant α, the spectrometer output function $R(\lambda)$ would be the graybody spectrum

$$R(\lambda) = \frac{\alpha\varepsilon\tau C_1}{\lambda^5(e^{C_2/\lambda T} - 1)} \tag{2}$$

Assuming that the constants ε, τ, and α are independent of wavelength over the measurement range, a scaled spectrometer output function based on Eq. (2) can be written as

$$SR(\lambda) = E(\lambda,T) = \frac{1}{\lambda^5(e^{C_2/\lambda T} - 1)} \tag{3}$$

S is the adjustable scale factor accounting for the unknown constants. For source temperatures less than about 3000 K and wavelengths less than 1 μm, the following approximation is valid since the term $\exp(-C_2/\lambda T) << 1$:

$$SR(\lambda) = E(\lambda,T) = \frac{e^{-C_2/\lambda T}}{\lambda^5(1 - e^{-C_2/\lambda T})} \cong \frac{e^{-C_2/\lambda T}}{\lambda^5} \tag{4}$$

Taking natural logarithms of both sides of Eq. (4) and rearranging gives

$$\ln\left(\frac{1}{\lambda^5 R(\lambda)}\right) = \left(\frac{C_2}{T}\right)\left(\frac{1}{\lambda}\right) + \ln S \tag{5}$$

Equation (5) is the basis of the data analysis method used here. For a spectrometer measurement function, $R(\lambda)$, a plot of $\ln(1/\lambda^5 R)$ vs $1/\lambda$ should be a straight line. Using a linear least-squares fit over the near-infrared wavelength measurement range adopted for the tests, 0.75 μm $\leq \lambda \leq$ 0.95 μm, the temperature T and the scale factor S can be obtained from the slope and the intercept, respectively. Alternatively, both sides of Eq. (5) can be multiplied by λ and the identification of the slope and the intercept will be interchanged. This equivalent equation was proposed by Ng *et al.*[17,18] for temperature analysis using a multiwave pyrometer.

Figures 4(a–c) show the near-infrared range spectrometer data taken for SiC-ground PSZ at increasing grinding downfeeds. The top frame in each plot is the spectrometer output function, $R(\lambda)$, for the grinding conditions indicated while the bottom frame shows the least-squares fit (solid line) according to Eq. (5). The solid curve through the $R(\lambda)$ plot is the fitted blackbody curve for the temperature and scale factor determined. Similar plots were obtained for other grinding conditions used in this study. The results for the source temperatures are summarized in Table I. Since no physical significance can be attached to the scale factors, these are not shown. For a given set of grinding conditions, the four to five temperature values reported in Table I correspond to grinding PSZ workpieces with different thicknesses.

The average temperatures in Table I are on the order of 3000 K for all conditions. No major trends for the effect of grinding conditions on the temperature can be identified. There does appear to be a slight decrease in temperature when downfeed is increased at constant wheel speed (SiC and diamond wheels) or when wheel speed is increased at constant downfeed (SiC wheel). However, these changes are close to the measurement standard deviations. There was a large amount of scatter in the data for the diamond wheel at the lowest downfeed, 0.0025 mm. The intensities measured were weak in this case and there was considerable scatter in the spectral outputs. Figure 4(d) shows typical results for 0.0025 mm downfeed diamond grinding tests.

If the wavelengths or source temperatures are higher than those assumed for the approximation given in Eq. (4), the method based on Eq. (5) may not be valid. Nevertheless, the same general approach for temperature measurement can be used. The difference is that one can no longer use the linear form given in Eq. (5) for the data fit, and a nonlinear regression method must be used. A method for this is outlined in the Appendix.

V. Discussion

A number of important features emerge from the results presented here. First, the source temperature results shown in Table I were consistent when selected measurements were repeated using the visible (Ocean Optics S2000) spectrometer over the range 0.4 μm $\leq \lambda \leq$ 0.8 μm.[15] This gives us confidence that the temperatures measured are due to thermal sources as opposed to a triboluminescent source. The latter is expected to produce localized peaks somewhere in the spectral output. If these did occur in one or the other of the spectrometer measurement ranges, then evidence of this would be apparent in the spectral outputs, and the temperature values reported in Table I should also show corresponding variations. This was not observed.

The estimation of temperature based on Eq. (5), or the Appendix, produces an *effective* graybody source temperature defined by matching the measured spectrometer output spectra to blackbody

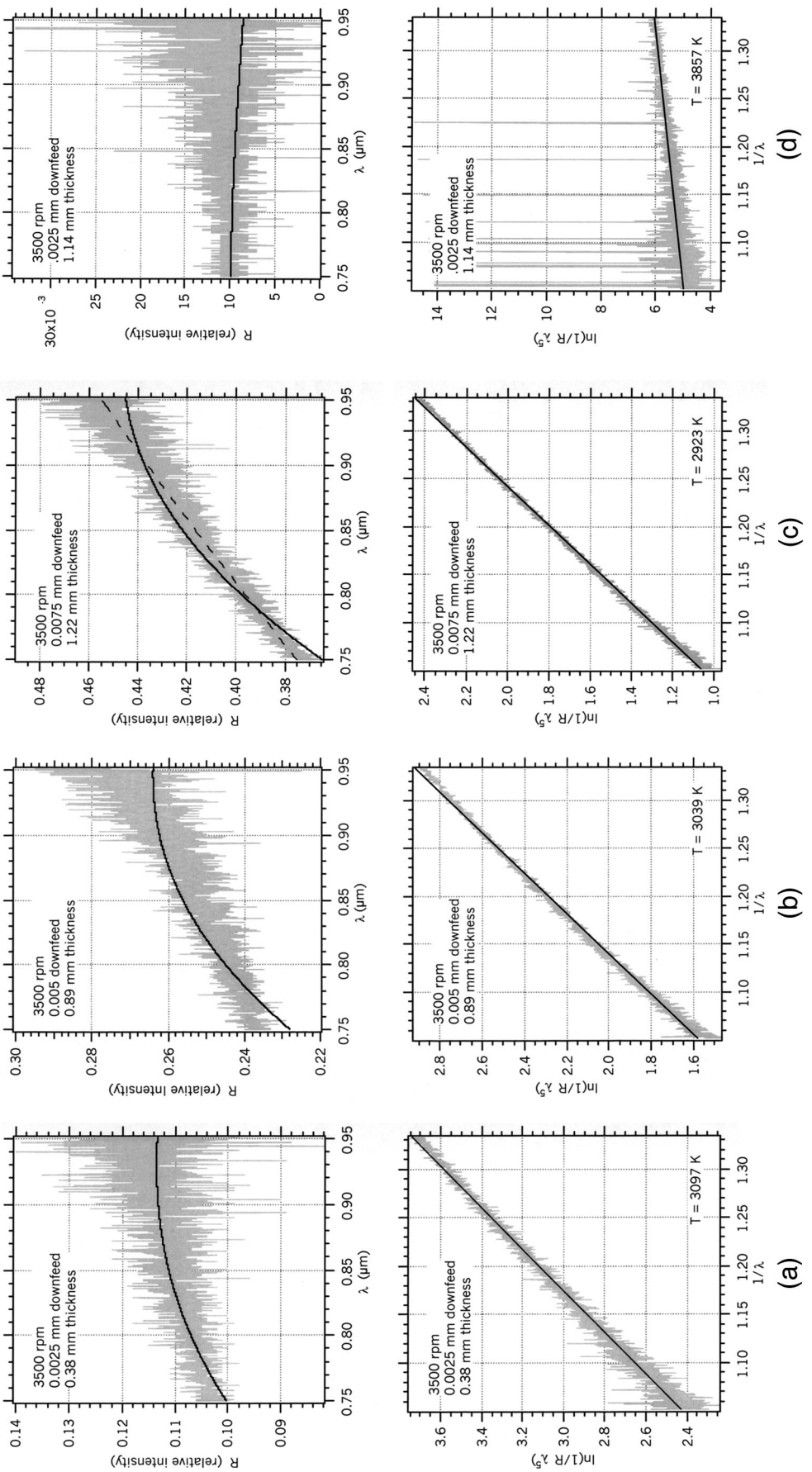

Fig. 4. Top frames show the measured spectrometer outputs, $R(\lambda)$ vs λ, and the best-fit blackbody curves (solid line). Bottom frames show the least-squares fits (solid lines) and effective temperatures obtained using Eq. (5). Wheel speed, downfeed, and sample thickness are indicated for each test. (a– c) SiC grinding wheel and (d) diamond grinding wheel.

Table I. Summary of the Results for the Temperature Measurements†

SiC grinding wheel temperatures					
Speed (rpm)	3500	3500	3500	4000	4500
Feed (mm)	0.0025	0.005	0.0075	0.005	0.005
MRR (mm^2/s)	0.375	0.75	1.125	0.75	0.75
T (K)	3094	3014	2923	3007	2952
	3095	3039	2970	3035	3013
	3069	3062	2972	3022	3020
	3097	3063	2956	3023	3003
		‡		3007	3008
Average	3089	3045	2955	3019	2999
Deviation	13.2	23.2	22.6	11.9	27.1
Diamond grinding wheel temperatures					
Speed (rpm)		3500	3500		3500
Feed (mm)		0.0025	0.005		0.0075
MRR (mm^2/s)		0.375	0.75		1.125
T (K)		3429	3191		2963
		3203	3021		2951
		3857	2969		2939
		3507	3060		2943
		3035			
Average		3406§	3060		2949
Deviation		313.4	94.8		10.6

†Grinding conditions given: wheel rpm (Speed), downfeed (Feed), material removal rate per millimeter of wheel width (MRR). The grinding table speed was 150 mm/s for all tests. ‡One test result gave a value of 2558 K. This appeared spurious and is not included in the average. §Signal strength was weak and scatter in the data for these grinding conditions was large.

curves over the wavelength measurement range. The scaling constant, S, and temperature, T, are adjustable parameters that provide the best least-squares regression fit. If a distribution of temperature exists within the source, then the effective temperature represents an average over this distribution. Because of the nonlinear dependence of the blackbody curves on temperature shown in Fig. 3, the averaging process will be biased with respect to temperature. The nature of this averaging process for grinding can be understood by using simulation calculations. Because of the localized contacts between grinding grits and workpiece material, there will be a distribution of grinding hot spots within the aperture of the spectrometer field of view. During the duration of a measurement, the hot-spot distribution varies in both spatial and time coordinates. It will be sufficient to consider a time-average, bimodal spatial variation of temperature such that, within the aperture, there is an area fraction f_h of hot-spot temperature, T_h, combined with an area fraction, $1 - f_h$, of temperature $T_b \leq T_h$, i.e., a cooler surface background temperature. The spectral power density received within the spectrometer aperture will then be proportional to the area-average function

$$E_{avg}(\lambda) = \varepsilon_h f_h E(\lambda,T_h) + \varepsilon_b(1 - f_h) E(\lambda,T_b) \quad (6)$$

where $E(\lambda,T)$ is given by Eq. (3). ε_h and ε_b are the hot-spot and background emissivities, respectively (assumed to be independent of λ). To determine an effective temperature, T, for this simulated distribution, set $R(\lambda) = E_{avg}(T)$ for specified values of T_h, f_h, T_b, ε_h, and ε_b, and then solve for T and S using linear least-squares regression, Eq. (5).

The wavelength range used for the simulation results shown in Fig. 5, 0.75 μm $\leq \lambda \leq$ 0.95 μm, was the same as that used for the spectrometer measurements. The hot-spot temperature was fixed at T_h = 3000 K. The background temperature was varied, 500 K $\leq T_b \leq$ 3000 K. Figure 5(a) shows the results for $\varepsilon_h = \varepsilon_b$ and varying area fraction, f_h, of hot spots. The effective temperature is the same as the hot-spot temperature if $T_b = T_h$ or if T_b is less than about one-third of T_h. In the intermediate range, the effective temperature depends on the percentage of hot-spot area (hot area). In any case, the effective temperature is always a lower limit for the hot-spot temperature. When compared with a spatial average temperature, $f_h T_h + (1 - f_h)T_b$, it is clear from Fig. 5(a) that the effective temperature is strongly biased toward the hot-spot temperature. This is a consequence of the highly nonlinear temperature dependence of blackbody radiation (Fig. 3). Similar results were obtained for the simulations shown in Fig. 5(b), where the emissivity ratio, $\varepsilon_b/\varepsilon_h$, was varied with f_h = 0.05 (5% hot spots). It should be noted that the form of the curves in Fig. 5 is not sensitive to the choice of the temperature T_h = 3000 K used for the simulations. Similar conclusions would be reached if, for example, simulations were run using T_h = 1500 K.

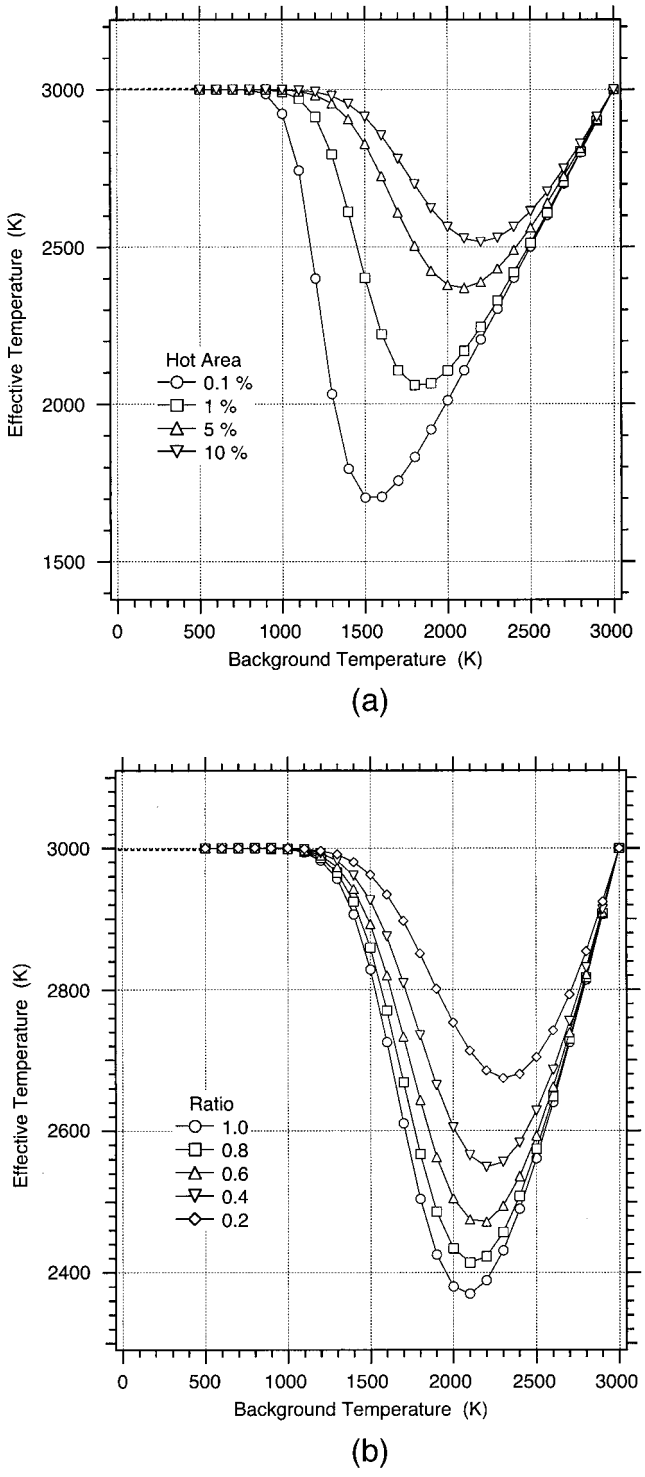

Fig. 5. Simulation results for determination of the effective temperature: (a) the area fraction of hot spots was varied as indicated and (b) the background:hot spot emissivity ratio was varied as indicated.

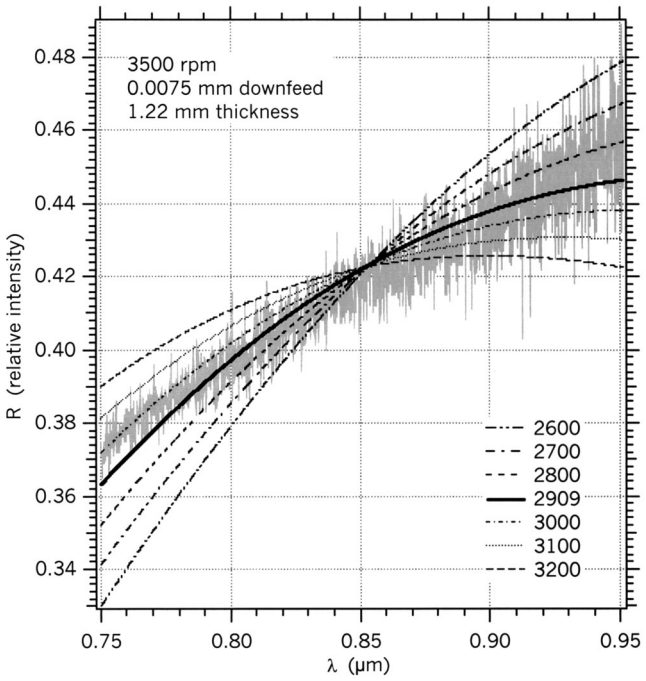

Fig. 6. Best-fit blackbody curves for a range of temperatures. The $R(\lambda)$ vs λ spectrometer data used are the same as those shown in Fig. 4(c).

Although we cannot determine the hot-spot area fraction or the background temperature for the experimental tests, the fact that excess *m* phase remains in the ground surfaces[14] indicates that the overall background temperature must be below the $m \rightarrow t$ transformation temperature at 1513 K (Fig. 1). For a reasonable estimate of grinding conditions, say background temperature on the order of 1000 K and 5% hot-spot area, Fig. 5 shows that the effective temperatures in Table I closely represent the grinding hot-spot temperature, $T_{h.}$

While the reproducibility of the temperature measurements summarized in Table I is quite good in almost all cases, it is pertinent to address the potential variability introduced by "shape matching" measured spectra with blackbody curves. Results for this are shown in Fig. 6. The $R(\lambda)$ curve shown in Fig. 4(c) is used for illustration. Best fits to the measured data were obtained using the nonlinear regression method discussed in the Appendix. For convenience, the $R(\lambda)$ data were represented by a second-order polynomial fit (dashed curve in Fig. 4(c)). The global best-fit curve is shown as the solid line in Fig. 6. The effective temperature obtained, 2909 K, differs from the value of 2923 K obtained in Fig. 4(c) using Eq. (5). Numerical differences introduced using the two regression schemes account for this small discrepancy. The remaining curves in Fig. 6 show the best-fit blackbody curves for a range of temperatures, ± 300 K, around 2909 K. These correspond to best-fit deviations larger than the minimum shown in Fig. A1. Based on the visual differences for curve matching seen in Fig. 6, and given the scatter in the measured $R(\lambda)$ data, it is apparent that the curve-matching strategy underlying the spectrometer data analysis method should produce effective temperatures that are reliable within a ± 300 K uncertainty band.

X-ray diffraction measurements made in a companion study[14] showed that the as-received PSZ samples contained ~10% of *m* phase. After grinding, the surface layer contained 16%–21% *m* phase, depending on the grinding conditions. Excess *m* phase in the ground-surface layer is the expected response because metastable *t* phase particles present in the as-received material will transform under the action of the grinding contact stresses.[13] In contrast, the SiC-ground chips did not contain any detectable *m* phase, and diamond-ground chips contained reduced amounts of *m* phase on the order of 4%–5%. This can be rationalized in terms of the thermomechanical history of the grinding chips. Since grinding chips are detached from the surface

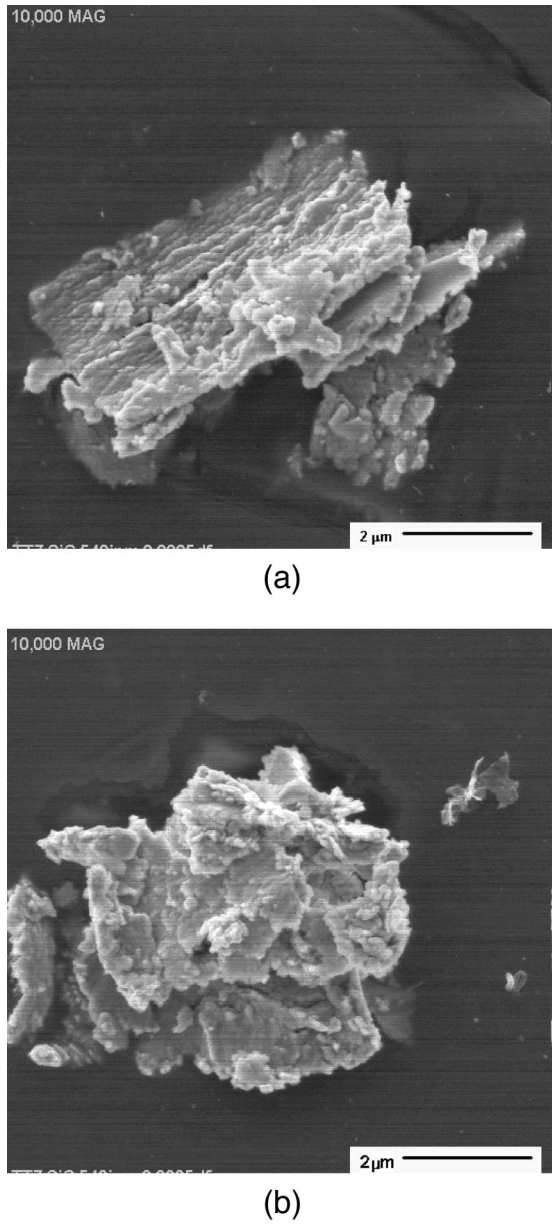

Fig. 7. SEM micrographs of grinding chips obtained using a SiC grinding wheel. The grinding conditions were 0.0127 mm downfeed and 2.91 mm^2/s material removal rate for both (a) and (b).

after their formation, the thermal response of the chips in a nominally stress-free state dictates their final $c + t + m$ phase content. The detached chips will be very hot, which we can assume to be on the order of the hot-spot temperatures of 3000 K (Table I). Contact with the grinding coolant will produce rapid quenching of the small chips. Based on the equilibrium phase diagram (Fig. 1), the $m \rightarrow t$ transformation will occur above 1513 K (1240°C) and at even higher temperatures, mixtures of *c* phase and liquid would be stable. However, it is not expected that the resolution or nucleation and growth transformations would occur because of kinetic constraints imposed by the very high heating/cooling rates. Such constraints would not affect the $m \rightarrow t$ martensitic reaction, and it is reasonable to conclude that the phase change occurring in grinding chips above 1513 K is the $m \rightarrow t$ reversion of the existing *t*-phase particles. Then, assuming that the particle size is small enough (subcritical) to suppress the M_s temperature below room temperature, there would be no *m* phase formed in nominally stress-free, detached grinding chips during cooling. This was the case for SiC-ground chips. Some residual *m* phase remained in diamond-ground chips, presumably

because the high thermal conductivity of diamond modifies the chip-temperature profile. The ground surfaces contain *m* phase since they are at temperatures below 1513 K. Their phase content is determined by the stress history, rather than thermal effects. Finally, the occurrence of *m* phase in the as-received samples is attributed to processing history and the grinding/polishing operations used to prepare the virgin surfaces.

As noted earlier, the individual amounts of *c* and *t* phases cannot be detected by X-ray measurements because of overlap of the diffraction peaks. Therefore, X-ray data do not reveal changes in the amount of *t* phase in the grinding chips, relative to the as-received material, that might have occurred during their thermomechanical history. Definitive evidence for the proposed scenario based on chip-temperature driven reversion of *m* phase in subcritial size *t*-phase particles would require TEM investigation of the microstructures present. Notwithstanding the difficulties in preparing TEM specimens from grinding swarf, this kind of study was beyond the scope of the present investigation.

In addition to causing the reversion of the *m* phase, very high temperatures would also facilitate the formation of mechanically soft, ductile grinding chips. Thermal softening effects are considered to be a primary contributing factor for the unique success of properly selected SiC grinding wheels for high material-removal rate, high *G* ratio of grinding MgO-PSZ ceramics.[16] Usual experience dictates that hard structural ceramics cannot be ground with common abrasives such as SiC because the high grinding forces must lead to excessive wear and/or damage of the grinding grit. Higher-cost diamond grinding must be used.

SEM observations of the PSZ grinding chips were reported in a companion study.[14] Typical results for SiC-ground chips are shown in Figs. 7(a) and (b), respectively. Ductilelike chip morpholgy, similar to metal machining, can be found on the chips as is seen in Fig. 7(a). Furthermore, the chips often show the granular/globular appearance seen in Fig. 7(b). Although not conclusive, the latter is suggestive of partial melting of the chip surface, consistent with very high chip temperatures. Similar features were found for diamond grinding wheels, and in this case long ductilelike chips were present. Presumably this is due to the sharper cutting edges presented by diamond grit compared with SiC grit. Even with the high hot-spot temperatures, diamond grit is a robust grinding media for PSZ, suggesting that the high thermal conductivity of diamond must prevent the grits from experiencing excessive thermal degradation.

VI. Summary and Conclusions

A spectrometer method was developed to measure the grit–workpiece interface temperatures for grinding 9 mol% MgO-PSZ. Advantage was taken of the fact that PSZ is semitransparent in the near-infrared and measurements were made using transmitted light. Effective temperatures on the order of 3000 K were obtained for the grinding conditions used. Simulations were made which showed that the effective temperatures measured are representative of the peak hot-spot temperatures reached during grinding. This is consistent with high grinding chip temperatures, which result from the very low thermal conductivity of PSZ. The high chip temperature causes reversion of the monoclinic phase to tetragonal phase in the grinding chips, whereas the ground surfaces contain excess monoclinic phase. Very high chip temperatures can also produce ductilelike grinding response. This effect appears to underlie the success for SiC grinding of PSZ components in high-volume production applications.

Appendix

When the approximation shown in Eq. (4) is invalid, the linear regression method corresponding to Eq. (5) cannot be used. In order to deal with this case, consider the general form for the least-squares deviation, Δ, given by

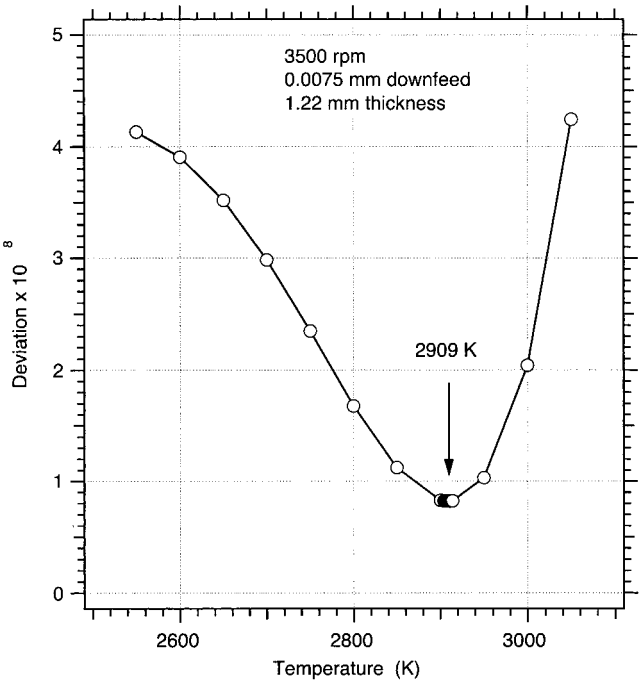

Fig. A1. Simulation results for deviation vs temperature.

$$\Delta(T,S) = \int (SR - E)^2 \, d\lambda \tag{A-1}$$

The integral is to be evaluated over the spectrometer wavelength measurement range. $R(\lambda)$ is the measured spectrometer function, S is the scaling factor, and $E(\lambda,T)$ is the blackbody function in Eq. (3). Minimization to obtain the best fit of the scaled spectrometer function to the blackbody curve must be done over a two-dimensional parameter space for S and T, hence,

$$\left(\frac{\partial \Delta}{\partial S}\right)_T = 0 \tag{A-2}$$

$$\left(\frac{\partial \Delta}{\Delta T}\right)_S = 0 \tag{A-3}$$

An explicit solution for T cannot be obtained; however, using Eq. (A-1), Eq. (A-2) can be solved explicitly for S.

$$S = \frac{\int ER \, d\lambda}{\int R^2 \, d\lambda} \tag{A-4}$$

Equation (A-4) is the best-fit value of S for any given value of T; therefore, we can reduce the problem to one-dimensional minimization for T. Substituting Eq. (A-4) into Eq. (A-1) gives

$$\Delta(T) = \int E^2 \, d\lambda - \frac{\left[\int ER \, d\lambda\right]^2}{\int R^2 \, d\lambda} \tag{A-5}$$

Equation (A-5) can be evaluated numerically for specified values of T. The required value of T is obtained for the minimum deviation. As an illustration, the spectrometer data shown in Fig. 4(c) were

analyzed using Eq. (A-5). For convenience, the spectrometer function $R(\lambda)$ was represented by a second-order polynomial shown as the dashed line in Fig. 4(c). After substituting the polynomial approximation for $R(\lambda)$ into Eq. (A-5), the integrals were evaluated numerically using standard mathematical integration routines (Maple V). The results are shown in Fig. A1. The value of T obtained at the minimum point (arrow) is 2909 K. This can be compared to the value, 2923 K, obtained for the same data using the linear regression fit, Eq. (5). This small discrepancy is attributed to numerical differences arising between the two computational methods. Values of S and T obtained with deviations above or below the minimum at 2909 K correspond to the best-fit blackbody curves for these temperatures. These are shown in Fig. 6.

References

[1]S. Malkin and R. B. Anderson, "Thermal Aspects of Grinding: Part 1, Energy Partition," *J. Eng. Ind.*, **96**, 1177–83 (1974).

[2]H. L. Costa, V. C. Pandolfelli, and J. D. Biasoli de Mello, "On the Abrasive Wear of Zirconias," *Wear*, **203–204**, 626–36 (1997).

[3]M. V. Swain and R. H. J. Hannink, "Metastability of the Martensitic Transformation in a 12 mol% Ceria–Zirconia Alloy: II, Grinding Studies," *J. Am. Ceram. Soc.*, **72** [8] 1358–64 (1989).

[4]T. Ueda, K. Yamada, and T. Sugita, "Measurement of Grinding Temperature of Ceramics Using Infrared Radiation Pyrometer with Optical Fiber," *J. Eng. Ind.*, **114**, 317–21 (1992).

[5]B. Zhu, C. Guo, J. E. Sutherland, and S. Malkin, "Energy Partition to the Workpiece for Grinding of Ceramics," *Ann. Int. Inst. Prod. Eng. Res.*, 21–26 (1995).

[6]S. Kohli, C. Guo, and S. Malkin, "Energy Partition to the Workpiece for Grinding with Aluminum Oxide and CBN Abrasive Wheels," *J. Eng. Ind.*, **117**, 160–68 (1995).

[7]R. R. Hebbar, S. Chandrasekar, and T. N. Farris, "Ceramic Grinding Temperatures," *J. Am. Ceram. Soc.*, **75** [10] 2742–48 (1992).

[8]S. Chandrasekar, T. Farris, and B. Bhushan, "Grinding Temperatures for Magnetic Ceramics and Steel," *J. Tribol.*, **112**, 535–41 (1990).

[9]T. N. Farris and S. Chandrasekar, "High-Speed Sliding Indentation of Ceramics: Thermal Effects," *J. Mater. Sci.*, **25**, 4047–53 (1990).

[10]T. Ueda, A. Hosokawa, and A. Yamamoto, "Studies on Temperature of Abrasive Grits in Grinding—Application of Infrared Radiation Pyrometer," *J. Eng. Ind.*, **107**, 127–33 (1985).

[11]J. O. Outwater and M. C. Shaw, "Surface Temperatures in Grinding," *Trans. ASME*, 73–86 (1952).

[12]J. A. Griffioen, S. Bair, and W. O. Winer, "Global Studies of Mechanisms and Local Analyses of Surface Distress Phenomona," Institut National des Sciences Appliquees, Lyon, France, September 3–6, 1985.

[13]R. Stevens, Magnesium Elektron Publication No. 113, *Zirconia and Zirconia Ceramics*. Magnesium Elektron Ltd., Manchester, U.K., 1986.

[14]A. J. Shih, R. O. Scattergood, A. C. Curry, T. M. Yonushonis, D. J. Gust, M. B. Grant, and S. B. McSpadden, "Grinding of Zirconia Using the Dense Vitreous Bond Silicon Carbide Wheel," submitted to *J. Manuf. Sci. Eng.*

[15]A. C. Curry, "Methods of Measuring Flash Temperatures in the Grinding of MgO–PSZ"; M.S. Thesis. North Carolina State University, Raleigh, NC, 2001.

[16]A. J. Shih and T. M. Yonushonis, "High Infeed Rate Method for Grinding Ceramic Workpiece with Silicon Carbide Grinding Wheels," U.S. Pat. No. 6 030 277, 2000.

[17]D. Ng and G. Fralick, "Temperature Measurement of Ceramic Materials Using a Multi-wavelength Pyrometer," *NASA Tech. Memo.*, **208850** (1999).

[18]D. Ng, "Temperature Measurement of a Glass Material Using a Multi-wavelength Pyrometer," *NASA Tech. Memo.*, **107433** (1997).

[19]C. F. Grain, "Phase Relations in the ZrO_2–MgO System," *J. Am. Ceram. Soc.*, **50** [6] 288–90 (1967). □